

Design a Rate-Hysteresis Reduction Task-space Control on a Stewart Robotic Platform

Yung Ting, Tho Van Nguyen, Mohammad Yaseen Joo, Ping Che Lu

*Department of Mechanical Engineering, Chung Yuan Christian University, No.200, Chung Pei Rd'
Chung Li, 32023, Taiwan (Tel: +886 03-2654319; e-mail: yung@cycu.org.tw)*

Abstract: A task-space control scheme is established by a derived dynamic model on the end effector associated with a few sensors employed on the specific location mounted on top of the piezo-driven 6DOF Stewart robotic platform. As piezoelectric actuators are used on the legs to manipulate the platform following an assigned trajectory, various manipulating speeds in operating frequencies may appear, making it more challenging to deal with the rate-dependent hysteresis effect. Despite the development of an Inverse Preisach model, building a large amount of information to identify the hysteresis loop at the different operating frequencies is complex and time-consuming. In an experiment, a nearly linear relation between the displacement of the leg actuator and input voltage is found. Thus, a run-to-run (RtR) adaptation procedure embedded on an internal model control (IMC) incorporated with the exponentially weighted moving average (EWMA) method called RtR_EWMA, is proposed. By means of the derived discrete-time formation that automatically adjusts the variant relation between the input driving voltage and the output displacement of the leg actuators, an easy and efficient control scheme is achieved. Time saving in computation is also an imperative advantage on performing on-line control of a complex 6DOF Stewart robot. In an experiment, free-space manipulation and machining of various work parts with different stiffness are carried out. The proposed feedforward controller, which consists of the Inverse Preisach model and the RtR_EWMA, is demonstrated to be effective by the findings. The task-space computed torque control approach works noticeably better when combined with the feedforward controller than when used alone.

Keywords: 6DOF Stewart robotic platform, task-space control, EWMA, run-to-run Internal Model Control

1. INTRODUCTION

High-precision positioning system providing spatial manipulation becomes essential for miscellaneous applications in semiconductor, optics, biomedical sciences, etc. A piezoelectric actuator-driven 6DOF Stewart-type robotic platform employed on each leg is thus built (Ting et al., 2007). Kinematic and dynamic equations are derived by combining the Newton-Euler method and the Lagrange formulation (Lebret et al., 1993; Dasgupta; Mruthyunjaya, 1998). The task-space control method is proposed via the dynamic modeling of the robotic platform's end effector in conjunction with an online assessment of the end effector's pose by deploying six high-quality sensors in a specific area; As a result, the end effector can be controlled directly, thereby improving precision and efficiency. The piezoelectric actuator has an intrinsic nonlinearity called hysteresis. This can lead to significant positioning errors while manipulating protracted displacement (Jiles et al., 1984). An inverse Preisach model is a well-known method for dealing with nonlinear hysteresis (Ge et al., 1997; Yu et al., 2002; Novak et al., 2018). In an experiment, the weighting function $\mu(\alpha, \beta)$ is determined from the measurement of hysteresis loop and as computation by the first order reversal curve method. Complex data processing and measurement errors due to insufficient saturation and calculated negative values of the weighting function will degrade accuracy (Novak et al., 2018). Moreover, temperature rise, creep effect, and operating frequency will affect the hysteresis and complicate the problem of

establishing a hysteresis controller. A few of research works proposed similar ways of derivation of inverse model to deal with. However, mathematical modeling is complex and needs numerous experiments to identify the weighting function or parameters etc. Hence, it becomes difficult and time-consuming in practical use (Senjyu et al., 1998; Jung et al., 2000; Li, et al., 2019; Al Janaideh et al., 2020).

How to overcome the problem of rate-dependent hysteresis characteristics and executing online adaptation is demanding. EWMA is a statistical control approach and Run-to-Run (RtR) feedback controller widely used in semiconductor production processes due to its stability, simplicity, and robustness. This control approach may automatically optimize the connection between the recipe's input and output target resultant from process drift and environmental disturbance, ensuring that the target is reached (Ingolfsson and Sachs, 1993; Chen et al., 1999). An extended EWMA, the PCC (Predictor Corrector Control), with two terms of adaptation algorithm can further reduce the drifting error (Butler and Stefani 1994).

A modified discrete-time adaptive feedforward controller that combines the inverse Preisach model with the EWMA (Exponentially Weighted Moving Average) method mapped into an RtR-IMC (run-to-run Internal Model Control) structure is proposed. The computed-torque method has been popularly used in robot control, which needs no references addressed here. Based upon a planned trajectory, the computed torque was formed in the 6DOF Stewart robotic platform's task-space model, including the stiffness model in combination with a

PID error state feedback control is designed. Further combination of the feedforward and the computed-torque-based model reference control is proposed and carried out free-space manipulation and machining on various work parts such as glass, and aluminum to verify and evaluate its performance.

2. KINEMATIC AND DYNAMIC MODELING

The 6-DOF Stewart platform is a parallel mechanism depicted in Figure 1. In this manipulator, the spatial motion of the movable platform is generated by five pieces of stack-type PZT actuators connected in series employed on each of the six legs, which provides about 60μm stoke in each leg. Each leg connects to the base of the platform and the mobile platform by flexural joints at points B_i and $P_i, i=1, 2, \dots, 6$, respectively. In order to examine the kinematics of the manipulator, frame $\{B\}$ and frame $\{P\}$ are fastened to the stationary and mobile platforms at points B_C and P_C , respectively. Coordinate systems of frame $\{B\}$ and frame $\{P\}$ are chosen so that the x -axis is perpendicular to the vectors B_1B_6 and P_1P_6 , respectively. The vector B_i describes the position of each joint located at the regular hexagon's apex concerning the frame $\{B\}$. Vector P_i describes the position of each joint concerning the frame $\{P\}$. The circumscribed lower and upper circles' radii are given by r_B and r_P , respectively. The structural angles on the fixed platform and the movable platform are represented as α_B and α_P that gives $\alpha = \alpha_B = \alpha_P = 0.012\pi$ subsequently. The angle λ_i between $B_C B_i$ and axis x_B , and the angle Λ_i between $P_C P_i$ and axis, x_P is defined as

$$\lambda_i = \left[\frac{\pi}{3} - \frac{\alpha}{2}, \frac{\pi}{3} + \frac{\alpha}{2}, \pi - \frac{\alpha}{2}, \pi + \frac{\alpha}{2}, \frac{5\pi}{3} - \frac{\alpha}{2}, \frac{5\pi}{3} + \frac{\alpha}{2} \right]^T \quad (1)$$

$$\Lambda_i = \left[0 + \frac{\alpha}{2}, \frac{2\pi}{3} - \frac{\alpha}{2}, \frac{2\pi}{3} + \frac{\alpha}{2}, \frac{4\pi}{3} - \frac{\alpha}{2}, \frac{4\pi}{3} + \frac{\alpha}{2}, 0 - \frac{\alpha}{2} \right]^T \quad (2)$$

The position of the point P_C concerning frame $\{B\}$ is defined as $P = [P_x \ P_y \ P_z]^T$, and The movable platform's orientation is defined by the rotation matrix R_P presented in Appendix I. Employing each of the six capacity sensors on the assigned location of a sensor holder shown in Figure 2, measurement of the pose of the center point on the moving platform is achieved. Using the measure on the end effector, calibration and error compensation is carried out, which can also support the control of the end effector (Ting et al., 2007).

The dynamic equation on the end effector is described by

$$(h)\ddot{h} + C(h, \dot{h})\dot{h} + G(h) + \mathcal{F}_{ext} = \mathcal{F} \quad (3)$$

where $h = [x, y, z, \theta_x, \theta_y, \theta_z]^T$ denotes the platform's nominal centre of mass stance; $M(h), C(h, \dot{h}), G(h)$ signifies the inertial, Coriolis and centrifugal, and gravity terms, respectively; \mathcal{F} implies the vector of generalized forces of the robotic platform. The terms of $M(h), C(h, \dot{h}), G(h)$ are the combination of the dynamic equation of the platform and the six legs in a closed form given by

$$M(h) = M_{mp} + \sum_{i=1}^6 \bar{M}_i; C(h, \dot{h}) = C_{mp} + \sum_{i=1}^6 \bar{C}_i; G(h) = G_{mp} + \sum_{i=1}^6 \bar{G}_i \quad (4)$$

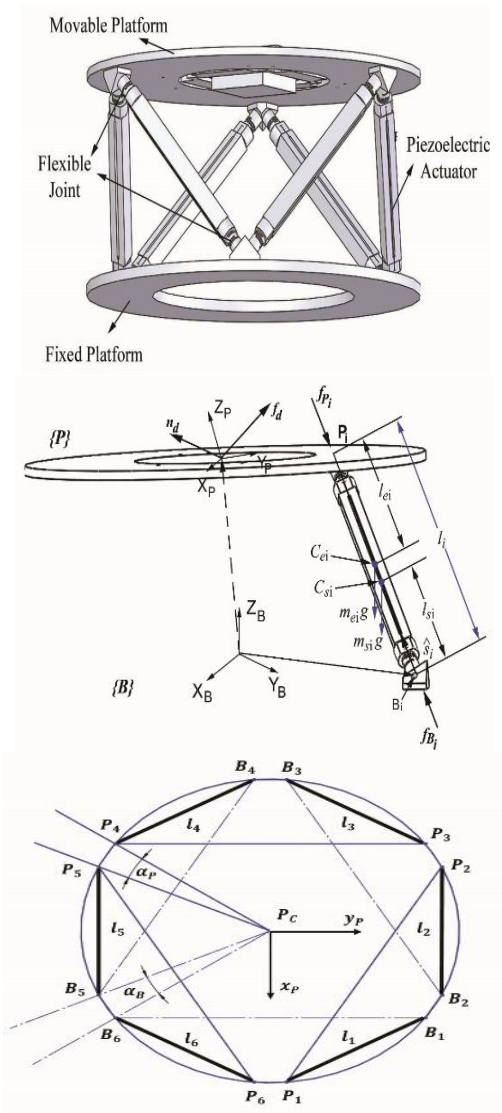


Fig. 1. Geometric drawing of Stewart-type platform.

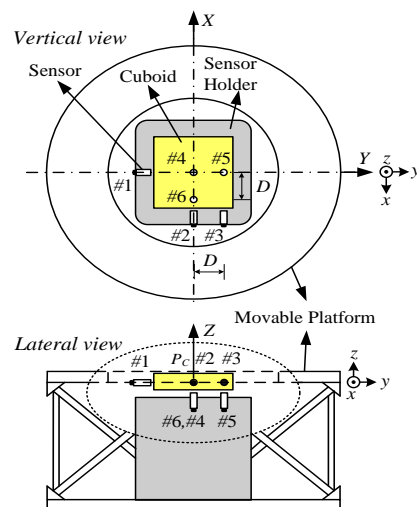


Fig. 2. Measure of end-effector with 6 sensors on sensor holder where the platform is associated by.

$$M_{mp} = \begin{bmatrix} m_{3 \times 3} & 0_{3 \times 3} \\ 0_{3 \times 3} & I_{mp} \end{bmatrix}_{6 \times 6}; C_{mp} = \begin{bmatrix} 0_{3 \times 3} & 0_{3 \times 3} \\ 0_{3 \times 3} & \omega \times I_{mp} \end{bmatrix}_{6 \times 6}; G_{mp} = \begin{bmatrix} -mg \\ 0_{3 \times 1} \end{bmatrix}_{6 \times 1}$$

and ω_B : angular velocity of legs; I_B : moment of inertia.

Where the legs are associated by

$$\bar{M}_i = J_i^T M_i J_i; \bar{C}_i = J_i^T M_i \dot{J}_i + J_i^T C_i J_i; \bar{G}_i = J_i^T G_i, \bar{F}_i = J_i^T F_i$$

and J is the Jacobian.

Considering the robotic platform executing machining on the solid work parts presumed as in interaction with a stiff environment. Under the condition that the robot stiffness is higher than that of the material parts, the work parts would experience deformation in translation and orientation. Assuming the equivalent interaction force behaves as a linear spring, it can be estimated by (Salisbury, J. K. (1980).

$$F_{ext} = K_e(h - h_e) \quad (5)$$

where K_e is matrix with diagonal elements that describes the stiffness of the work parts; h_e denotes the undeformed pose of the work parts while in contact with the cutting tool.

A brief derivation of the kinematic and dynamic model is described in Appendix I.

3. HYSTERESIS FEEDFORWARD CONTROLLER

Hysteresis is a natural characteristic of nonlinearity existing in piezoelectric materials. The PZT actuator has the disadvantage of rate-dependent hysteresis caused by temperature and creep (Jung and Gweon, 2000; Ting et al., 2011). The temperature effect is negligible, for the temperature is maintained at room temperature during the experiment in this study. The hysteresis loop is variable and rounder when the rate of input driving voltage is increased. In Figure 3, the hysteresis of a leg actuator of the robotic platform is variant for different manipulating speeds in terms of operating frequency (Hz) or sampling intervals. The dynamic Preisach model was created using the conventional Preisach model provided by

$$\begin{aligned} q(t) &= \iint_{\alpha \geq \beta} \mu_0(\alpha, \beta) \gamma_{\alpha\beta}[u(t)] d\alpha d\beta \\ &\quad + \iint_{\alpha \geq \beta} \frac{du}{dt} \mu_1(\alpha, \beta) \gamma_{\alpha\beta}[u(t)] d\alpha d\beta \quad (6) \\ &= q(t)^{CPM} + \iint_{\alpha \geq \beta} \frac{du}{dt} \mu_1(\alpha, \beta) \gamma_{\alpha\beta}[u(t)] d\alpha d\beta \end{aligned}$$

where $\mu_0(\alpha, \beta)$ and $\mu_1(\alpha, \beta)$ represents the static and dynamic components of hysteresis of the weighting function; $\gamma_{\alpha\beta}$ is defined as having a value of either 0 or 1; the superscript ‘‘CPM’’ denotes the outcomes calculated using the traditional Preisach model. Additionally, the ability to eliminate is used to lessen errors brought on by incorrect local extreme points. Without further description in this article, an inverse algorithm using the numerical method for the dynamic Preisach model was developed in our previous research work (Ting et al., 2011). While building an Inverse Preisach model represented with an operator Γ^{-1} , the input voltage and output displacement would appear to have a nearly linear relation. However, a slight deviation exists from the actual value; an approximately linear relation is found and shown in Figure 4 for the chosen examples of (0.1, 1.0, 10, 20, 40, 50) Hz, respectively. As observed, the input/output relation is variant for different

operating frequencies. That is, measurement of the hysteresis loop to search for the weighting function $\mu(\alpha, \beta)$ under numerous operating frequencies is necessary; however, it is very time-consuming and infeasible in practical use. Hence, an approach such as the EWMA method to cope with a varying linear connection between the output and input is proposed. The linear relation that an equation can express $Y_n = \rho_n X_n + \delta_n + d_n$, where ρ_n is the system gain or slope; δ_n is the system biased or offset; d is the disturbance or noise. Assuming no disruption is involved, the corresponding coefficients of the found linear relation for different operating frequencies are shown in Figure 4 and are listed in Table 1.

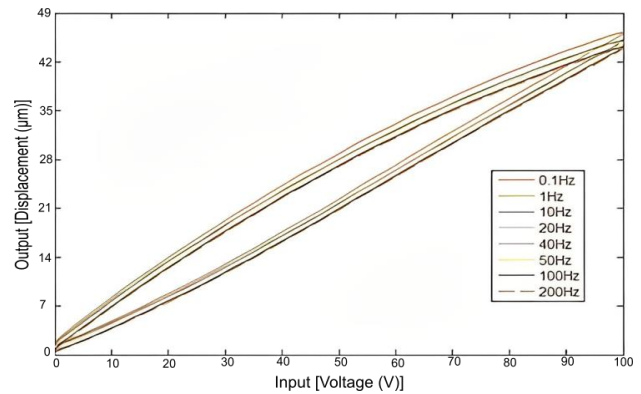


Fig. 3. Rate-dependent hysteresis.

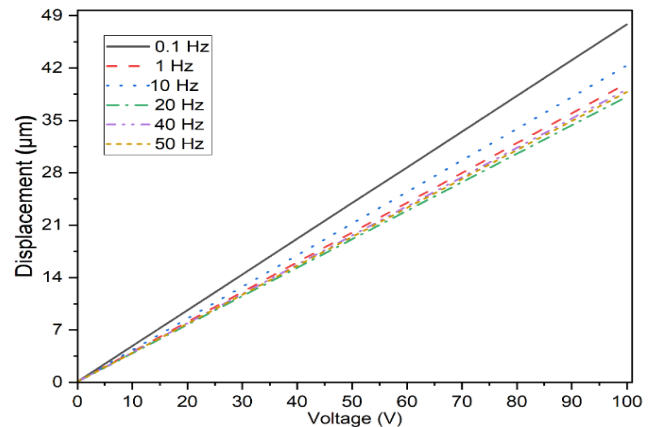


Fig. 4. Displacement vs input voltage.

Table 1. Coefficients of a linear relationship.

Frequency Hz	Bias α	Gain slope β
0.1	0.682	0.1282
1	0.5694	0.1262
10	0.6035	0.1256
20	0.5440	0.1253
40	0.5580	0.1248
50	0.5530	0.1244

The hysteresis feedforward Control Scheme is illustrated in Figure 5. Using the inverse Preisach model denoted by Γ^{-1} considerably reduces the PZT actuator's nonlinear hysteresis. EWMA and its extended PCC methods are designed to deal with the inconsistent relation between the leg's displacement and the driving voltage due to variant operating frequencies.

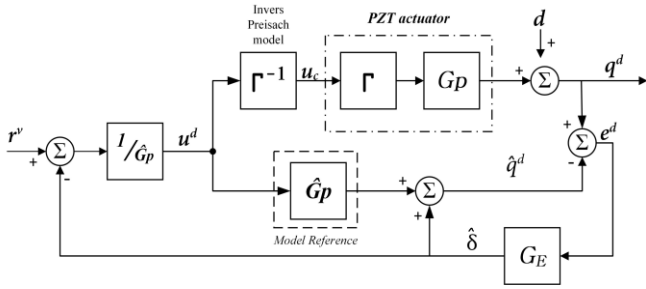


Fig. 5. Hysteresis Feedforward Control Scheme.

The EWMA or PCC controller G_E is integrated into an Internal Model Control (IMC) structure, where r^v is the input driving voltage and \hat{q}^d is the estimated actuator's leg displacement corresponding to the X_n and Y_n respectively in the linear form. Via the adaptively tuned gain represented by the transfer function \hat{G}_p approaching the actual gain G_P , an appropriate driving voltage is applied to obtain the actual output displacement q^d reaching the target value T .

Appendix II presents the developed discrete-time EWMA and PCC controller and their performance verification of dealing with step and ramp disturbance d .

To examine the performance of a feedforward controller on a leg actuator, an assigned trajectory example with arbitrarily chosen manipulation speed in terms of operating frequencies (0.1, 1.0, 10) Hz, which is usually practicable in nanoscale manipulating rate, is given below.

$$\begin{cases} q(t) = 1.95 * t * t_f & \text{when } 0 \leq t \leq 2/t_f \\ q(t) = 24 + 20 \sin(2\pi f_c t - 8\pi/q) & \text{when } 2/t_f < t \leq 22/t_f \end{cases}$$

Note that to manipulate the same trajectory, the auxiliary factor is assigned by $t_f = 1, 10, 100$ for the case of operating frequency (0.1, 1.0, 10) Hz, respectively. Thus, the period (22, 2.2, 0.22) seconds differs for each case (0.1, 1.0, 10) Hz. MATLAB is used to run the inverse Preisach hysteresis algorithm with EWMA or PCC method embedded in the LabVIEW. Optimal weighting factors for EWMA and PCC controllers are selected to be $\omega_1 = 0.252$ and $\omega_1 = 0.252$, $\omega_2 = 0.011$, respectively, in reference to (Ingolfsson & Sachs 1993; Hunter 1986). Considering the desired trajectory with a chosen frequency is $f_c=0.1$ Hz as the reference-based operation frequency in search of the weighting function of the inverse Preisach model, the gain $\hat{\rho}$ of the estimated model \hat{G}_p is determined as $\hat{\rho} = 0.1262$. The inverse Preisach hysteresis (invhys) model, the inverse Preisach hysteresis model + EWMA (invhys-EWMA), and the inverse Preisach hysteresis model + PCC (invhys-PCC), three types of control methods are applied in experiment respectively. The measured results are shown in Figures 6~8, and the tracking error calculated by Root-Mean-Square Error (RMSE) and is listed in Table 2.

Table 2. Tracking error (nm) vs operating frequency.

Controls	frequency		
	0.1 Hz	1 Hz	10 Hz
Invhys	127.039	232.143	504.539
Invhys+EWMA	103.086	117.305	191.409
Invhys+PCC	80.5	81.783	156.25

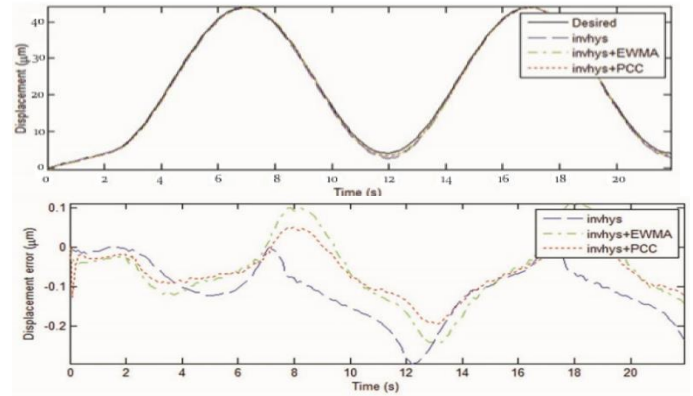


Fig. 6. Tracking performance and tracking error – 0.1 Hz.

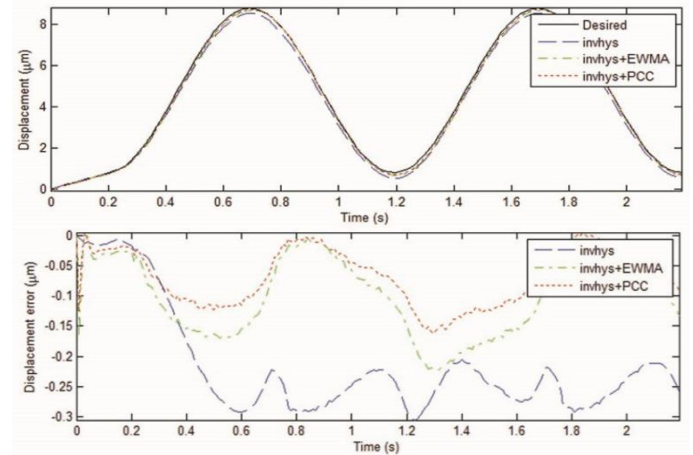


Fig. 7. Tracking performance and tracking error – 1.0 Hz.

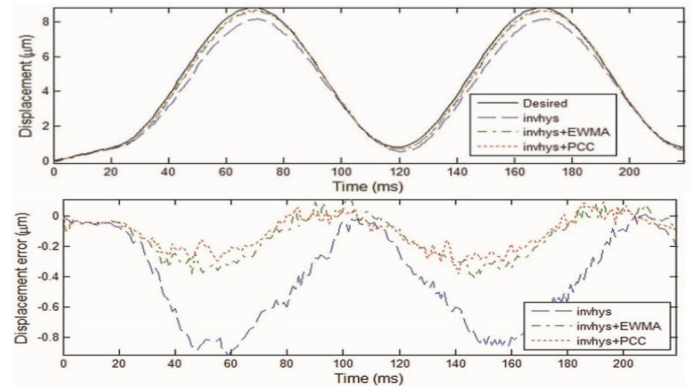


Fig. 8. Tracking performance & error – 10 Hz.

As expected, the EWMA method helps reduce error, and the PCC is superior to the others because the PCC acts as an integrator plus a double integrator that can effectively decrease error. Also, the error in the cases of 1.0Hz and 10Hz is deficient because 0.1Hz is the reference-based operation frequency to determine the inverse Preisach model's weighting scheme.

4. TASK-SPACE CONTROL SCHEME

The task-space control with a feedforward controller is illustrated in Figure 9. The 6DOF Stewart-type platform's dynamic equation involves the interaction force \mathcal{F}_{ext} from the environment stiffness described in (5). The generalized forces

of the robotic platform with the task-space stiffness controller constructed with a computer torque method and an error state feedback PID with gains (k_p, k_I, k_v) , named position tracking P controller, is given by

$$\mathcal{F} = M(h)\ddot{h}_d + C(h, \dot{h})\dot{h} + G(h) + k_v\dot{\tilde{h}} + k_p\tilde{h} + k_I \int \tilde{h} + K_e(h_d - h_e) \quad (7)$$

where $\tilde{h} = h_d - h$ is the tracking error.

Substituting (7) into (3) yields

$$M(h)\ddot{\tilde{h}} + k_v\dot{\tilde{h}} + (k_p + K_e)\tilde{h} + k_I \int \tilde{h} = 0 \quad (8)$$

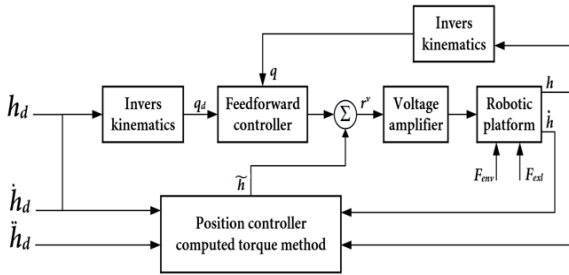


Fig. 9. The task-space stiffness control with feedforward controller.

The additional integrator k_I is helpful to reduce errors caused by model inaccuracy and disturbance, ideally achieving zero tracking position error. Gains in PID are attained using the Ziegler-Nichols method while searching out the ultimate time T_u as well as ultimate gain K_u via the Relay feedback test method (Astrom 1995). The found gains can be used as an initial trial to search for optimal gain in the later process of utilizing a genetic algorithm based on the minimization of ITAE (Integral-Time Absolute Error) error criteria, defined as

$$F_{cost} = \int_0^{t_{span}} (a_1 t |\dot{\tilde{h}}| + a_2 \eta_c^2) dt \quad (9)$$

where a_1 and a_2 are the weights chosen by the method described in reference (Zamani et al., 2009; Maiti et al., (2008) $\eta_c = k_v\dot{\tilde{h}} + k_p\tilde{h} + k_I \int \tilde{h}$. Table 3 provides the allocated genetic algorithm parameters. The gains are found and expressed with matrix form as $\text{diag}(k_v) = [(9.4017, 9.1688, 9.7290, 6.5998, 7.4715, 8.9556) \times 10^{-6}]$, $\text{diag}(k_I) = [(2.4727, 2.4114, 2.5587, 1.7358, 1.9650, 2.3553) \times 10^{-6}]$, and $\text{diag}(k_p) = [(0.0261, 0.0254, 0.027, 0.0183, 0.0207, 0.0248) \times 10^{-6}]$. $\text{diag}(k_I) = [(2.4727, 2.4114, 2.5587, 1.7358, 1.9650, 2.3553) \times 10^{-6}]$, and $\text{diag}(k_I) = [(0.0261, 0.0254, 0.027, 0.0183, 0.0207, 0.0248) \times 10^{-6}]$. Since the robotic platform works on a rigid surface with large stiffness, it is assumed $\text{diag}(K_e) = \text{diag}(k_p)$ and with the integrator k_I , the steady force exerted on the work parts is reduced (Lewis et al., 2003). Besides the robotic platform, There are two power amplifiers with three channels. (Piezomechanik, SVR-500/3) for PZT stack actuators (AE0505D18F, 6.5mm x 6.5mm x 18mm package, 150V), Lion precision capacity displacement sensors (Probe model: C6-D, Driver Model: DMT22, for large-stroke the sensitivity of 50 μ m is 2.2 μ m and the sensitivity for fine-stroke of 10 μ m is 0.4nm, Analog Output: $\pm 10V$), OptoForce 6-axis force/torque sensor (HEX-70-CE-2000N, Nominal capacity: $F_{xy} = \pm 300 N$, $F_z = 2000 N$, $T_{xy} = 15 Nm$, $T_z = 10 Nm$), A PC-

based control system, NI DAQ cards (NI PCI 6229, four 16-bit analogue outputs, 833 kS/s), and a diamond cutting tool (Rockwell diamond hardness indenter). As shown in Figure 10, the diamond tool is attached to the xyz flexural stage to make surface contact with the sample work parts. Coarse adjustment is made manually first, and then a fine adjustment is carried out by controlling the xyz stage until a small pulse appears on the force sensor.

Table 3. Genetic algorithm Parameters.

Items	Setting
Population type	Bit string
Population size	100
Selection function	Roulette
Crossover type	Two-point crossover
Crossover fraction	0.9
Mutation function	Uniform
Mutation rate	0.03
Weights	$a_1 = 0.998, a_2 = 0.002$

Table 4. Material properties of the robotic platform.

Properties	Symbol	Value(unit)
Moving platform mass	m_{mp}	1.195(g)
Fixed leg mass	m_{si}	90.26(g)
Extensible leg mass	m_{ei}	73.62(g)
Moment of Inertia of the Moving Platform	I_{xx}	3.26x10 ⁷ (gmm ²)
	I_{yy}	3.26x10 ⁷ (gmm ²)
	I_{zz}	9.7x10 ⁶ (gmm ²)
Moment of inertia of the fixed leg	I_s	1.07x10 ⁵ (gmm ²)
Moment of inertia of the extensible leg	I_e	5.27x10 ⁴ (gmm ²)

Before executing the machining case study, a fundamental free-space manipulation with the position tracking controller given in (7) ~ (9), which neglects the environment stiffness (K_e) and the interaction force \mathcal{F}_{ext} , are examined first with the associated Inverse Preisach model, EWMA, and PCC method employed with the same (gain and weighting factor) coefficients in the leg actuator described above.

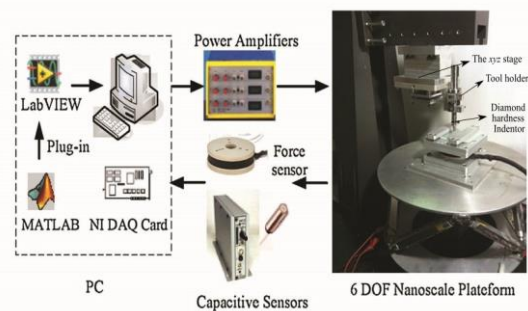


Fig. 10 Experimental Setup.

To ascertain the function of the proposed feedforward controller, including the Inverse Preisach model and the EWMA (PCC), experimental results are shown in Figures 11~16, 17~22, and listed in Tables 5~6 and 7~8 for operating different frequencies (0.1, 1.0, 10) Hz on the following arbitrarily chosen trajectory, case I and case II, respectively. Similarly, to manipulate the same trajectory, the auxiliary factor is assigned by $t_f = 1, 10, 100$ for the operating

frequency (0.1, 1.0, 10) Hz, respectively, and the corresponding time span is (25, 2.5, 0.25) seconds.

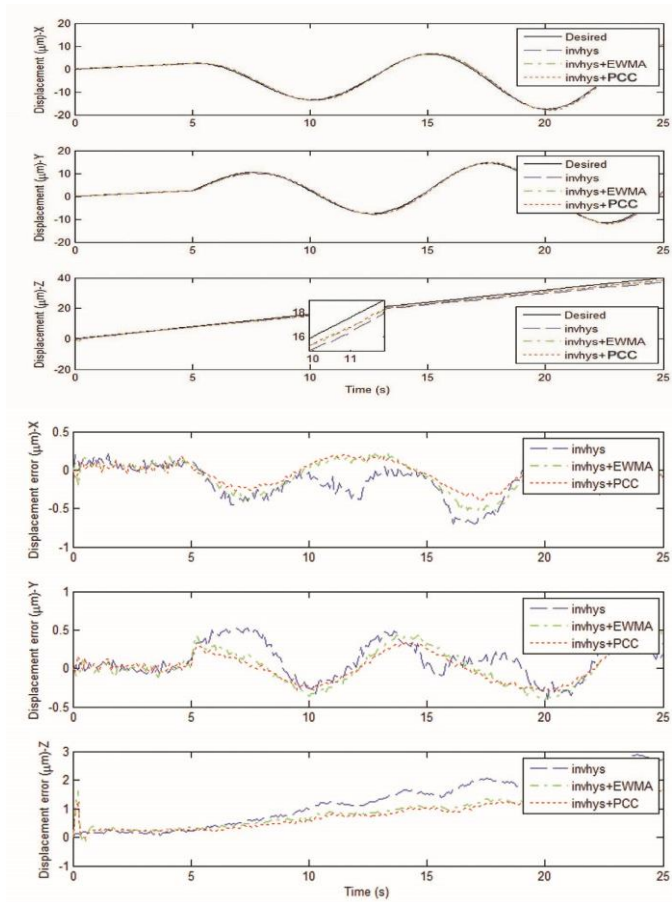


Fig. 11. Tracking performance & error –translation (0.1 Hz).

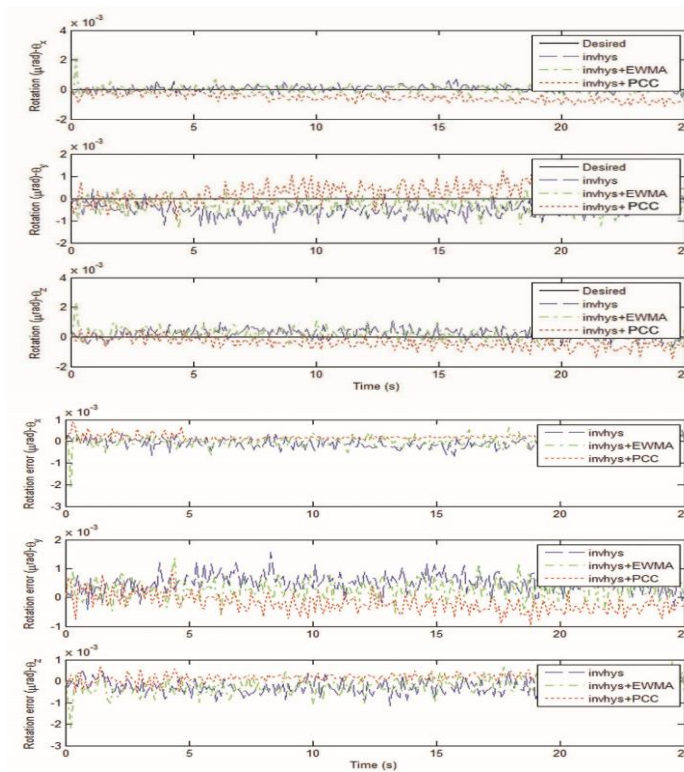


Fig. 12. Tracking performance & error – rotation (0.1 Hz).

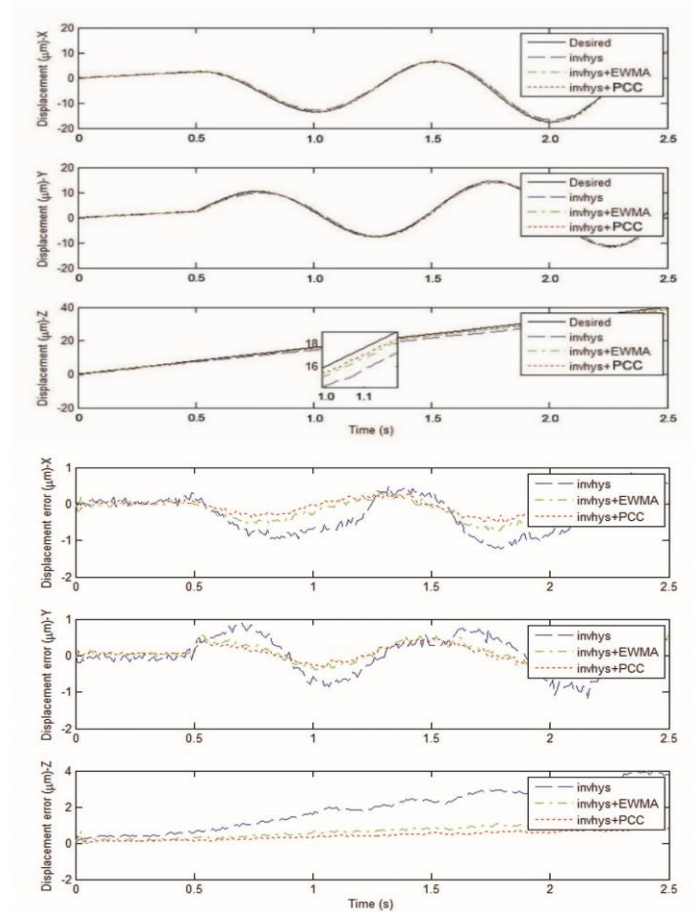


Fig. 13. Tracking performance & error – translation (1 Hz).

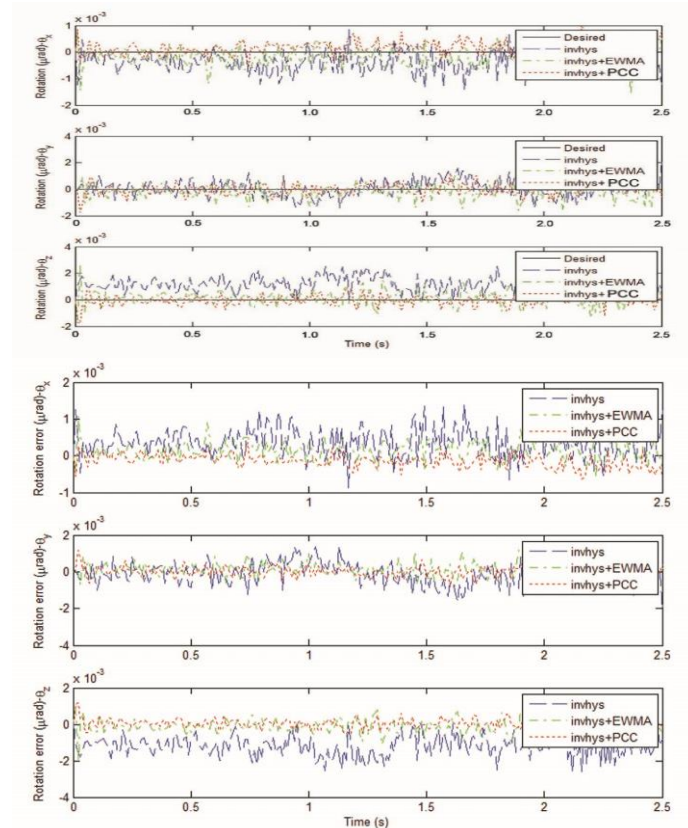


Fig. 14. Tracking performance & error – rotation (1 Hz).

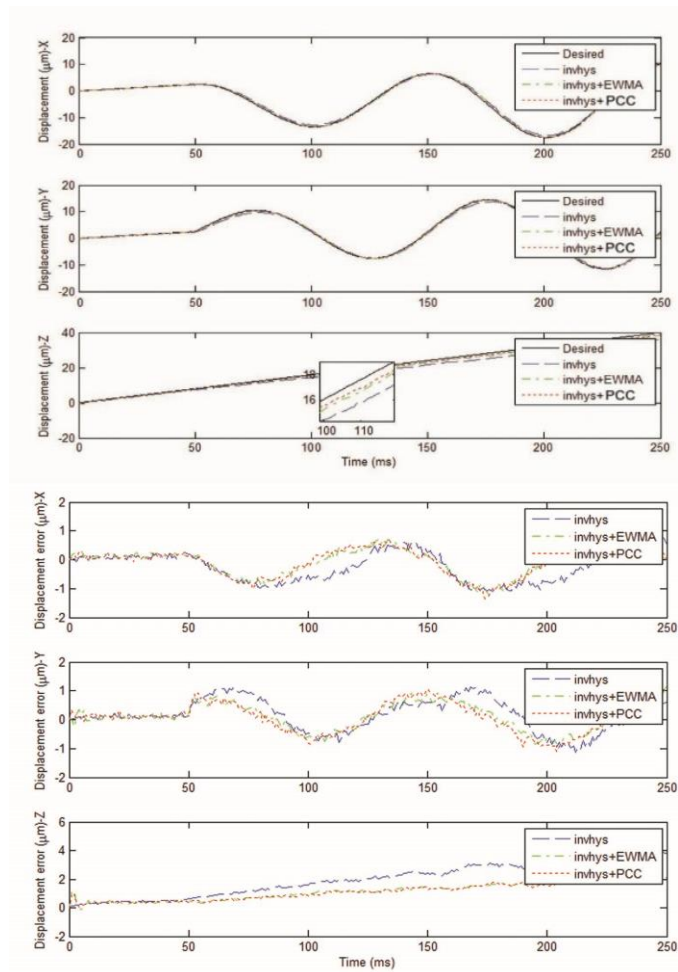


Fig. 15. Tracking performance & error – translation (10 Hz).

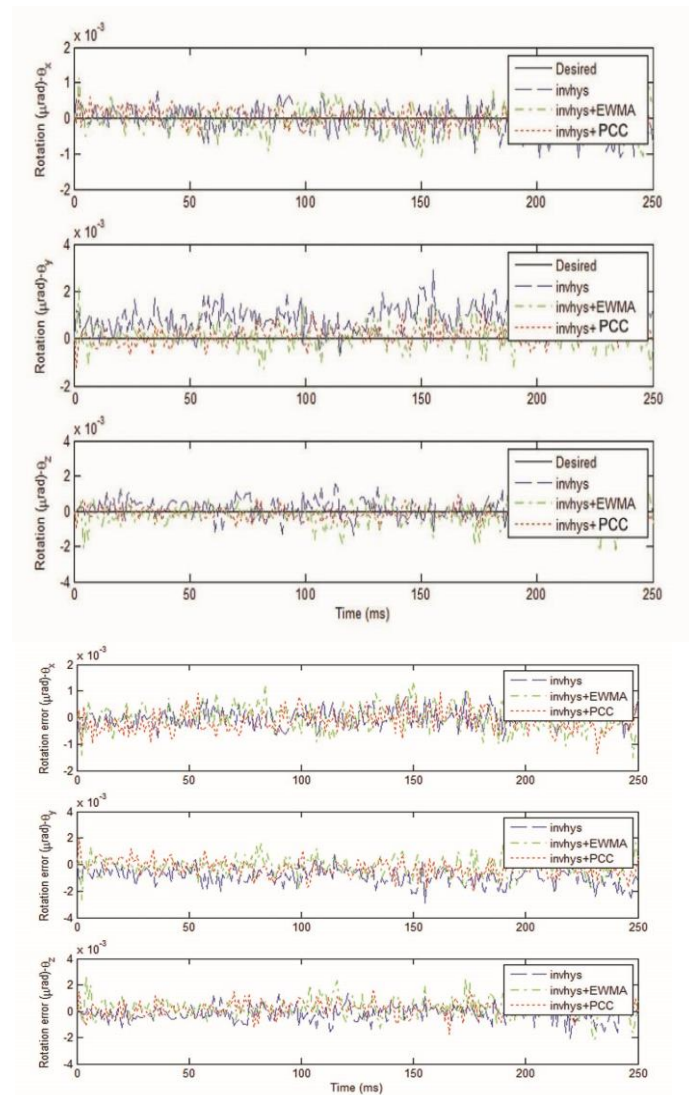


Fig. 16. Tracking performance & error – rotation (10 Hz).

Table 5. Translation tracking error (nm) vs operating frequency – X, Y, Z-axis.

Controls	frequency --- X			frequency --- Y			frequency --- Z		
	0.1 Hz	1 Hz	10 Hz	0.1 Hz	1 Hz	10 Hz	0.1 Hz	1 Hz	10 Hz
Invhys	282.595	660.4	786.138	281.976	544.273	768.052	1730.732	2560.3	3149.452
Invhys+EWMA	245.074	332.574	390.431	279.067	330.510	392.128	1093.873	838.412	998.552
Invhys+PCC	189.004	237.211	270.949	214.04	268.265	284.321	100.149	531.8	631.13

Table 6. Rotation tracking error (nrad) vs operating frequency – $\theta_x, \theta_y, \theta_z$ -axis.

Controls	frequency --- θ_x			frequency --- θ_y			frequency --- θ_z		
	0.1 Hz	1 Hz	10 Hz	0.1 Hz	1 Hz	10 Hz	0.1 Hz	1 Hz	10 Hz
Invhys	0.229	0.546	0.58	0.622	0.675	1.384	0.426	1.365	0.783
Invhys+EWMA	0.211	0.307	0.369	0.453	0.430	0.524	0.369	0.430	0.597
Invhys+PCC	0.201	0.241	0.287	0.369	0.397	0.429	0.259	0.298	0.325

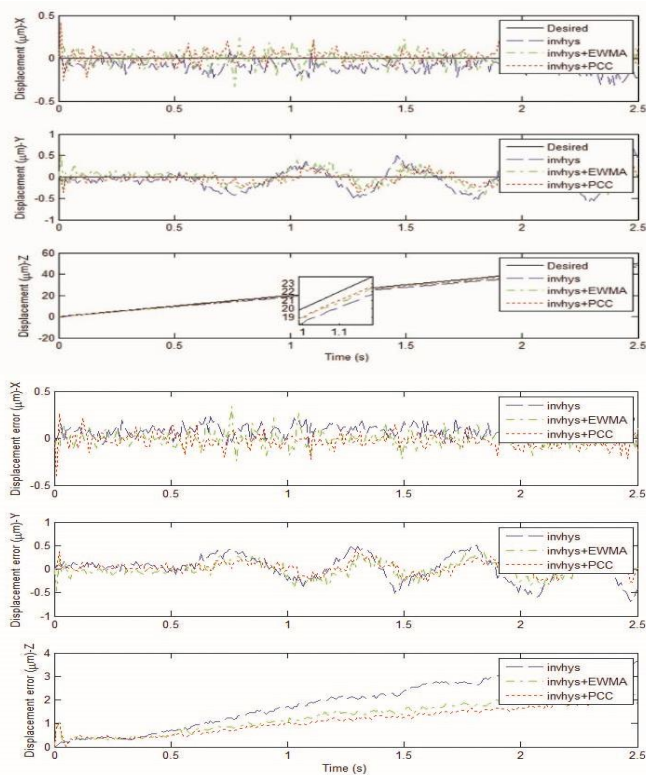


Fig. 19 Tracking performance & error –translation (1.0 Hz)

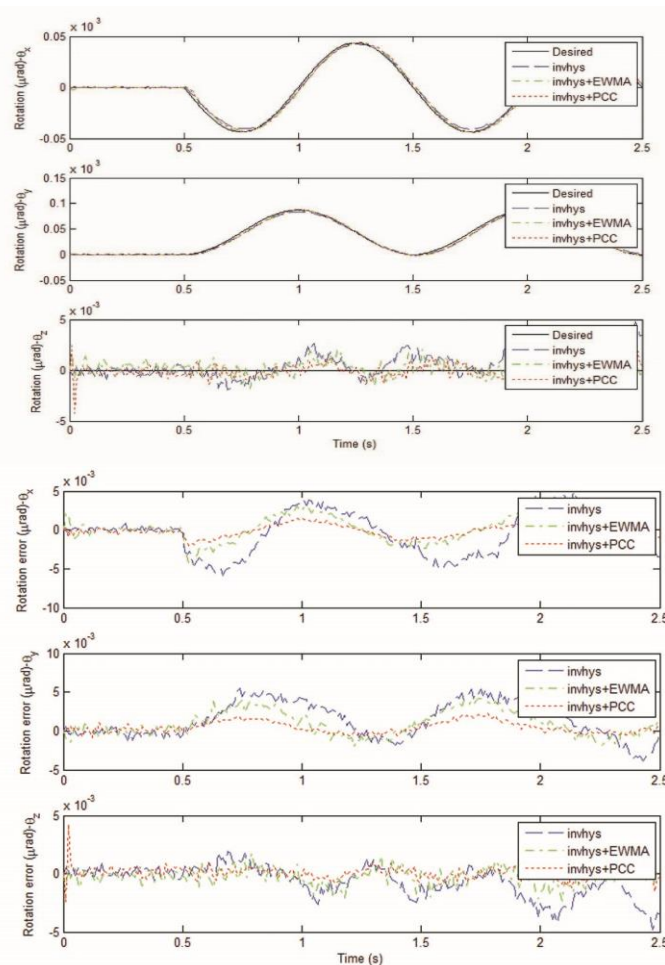


Fig. 20. Tracking performance & error – rotation (1.0 Hz).

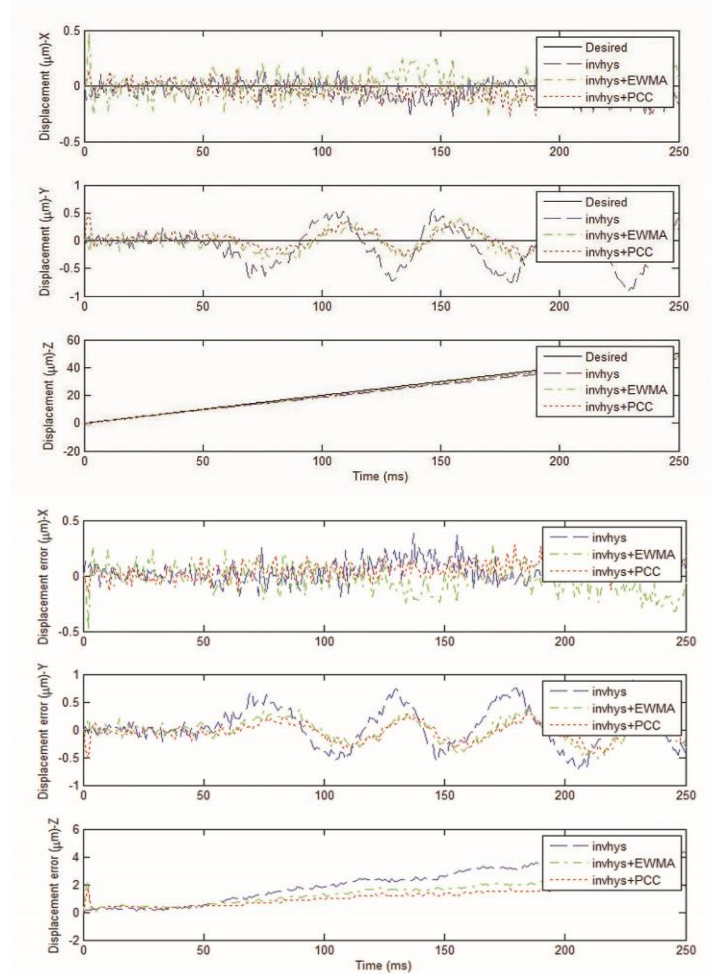


Fig. 21. Tracking performance & error –translation (10 Hz).

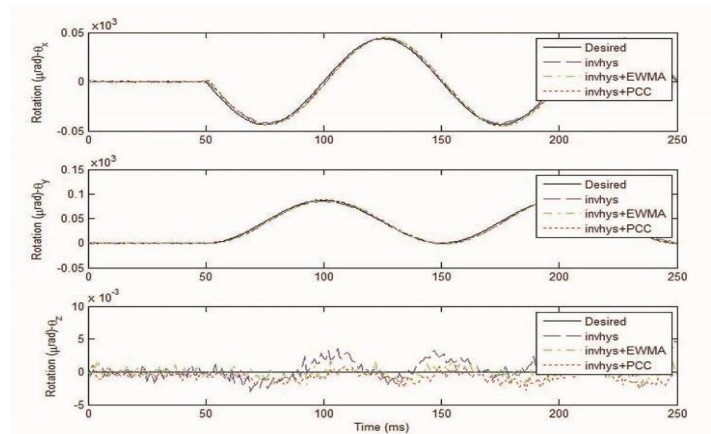


Fig. 22. Tracking performance & error – rotation (10 Hz).

Same outcomes as the above leg actuator case study are found. Combining the inverse Preisach model with the PCC yields the smallest RMSE error, which is superior to the others at the variant operating frequency. Since the inverse Preisach model with the PCC controller can achieve the best tracking performance, combining the position tracking (P) controller defined in (7) with the feedforward controller, named P/F controller, will be used for stiffness control. Therefore, the general task-space position tracking controller (P) alone will compare with the combined P/F controller. Also, to further

Table 7. Translation tracking error (nm) vs operating frequency – X, Y, Z-axis.

Controls	frequency --- X			frequency --- Y			frequency --- Z		
	0.1 Hz	1 Hz	10 Hz	0.1 Hz	1 Hz	10 Hz	0.1 Hz	1 Hz	10 Hz
Invhys	85.281	128.905	140.329	278.405	304.039	418.17	1537.291	2486.483	2888.631
Invhys+EWMA	75.235	85.442	128.691	149.682	183.826	224.769	991.101	1623.527	1812.541
Invhys+PCC	68.236	75.146	102.296	122.484	150.953	183.944	812.071	1366.833	1389.31

Table 8. Rotation tracking error (nrad) vs operating frequency – $\theta_x, \theta_y, \theta_z$ -axis.

Controls	frequency --- θ_x			frequency --- θ_y			frequency --- θ_z		
	0.1 Hz	1 Hz	10 Hz	0.1 Hz	1 Hz	10 Hz	0.1 Hz	1 Hz	10 Hz
Invhys	1.867	3.007	3.475	1.522	3.049	3.661	1.424	1.637	2.147
Invhys+EWMA	1.687	1.823	2.771	1.484	2.047	2.578	0.576	0.828	0.865
Invhys+PCC	0.791	0.917	1.351	1.398	1.431	2.101	0.513	0.54	0.689

verify the function capability of feedforward control, the operation frequency is chosen 1.0Hz on purpose, which is different from the reference-based frequency $f_c=0.1$ Hz. An arbitrarily chosen spiral trajectory for machining the work parts, including the selected glass (Gls) and aluminum (Al), is divided into three segments. The robotic platform moves along the X, Y, and Z-axis in the first segment, respectively. The second segment moves upward along the Z-axis and simultaneously moves sinusoidally along the X and Y-axes. The third segment returns to (origin) home position along the X, Y, and Z-axis. The trajectory in both translation and orientation is given below.

$$x(t) = \begin{cases} 5t * t_f & , 0 < t \leq 0.5/t_f \\ \left[-3.3 + \left(5 + \frac{8t * t_f}{5} \right) \sin \left(2\pi f_c t - \frac{\pi}{2} \right) \right] & , 0.5/t_f < t \leq 2.5/t_f \\ \left[5.7 - 5.7(t * t_f - 2.5) \right] & , 2.5/t_f < t \leq 3.5/t_f \end{cases}$$

$$y(t) = \begin{cases} 5t * t_f & , 0 < t \leq 0.5/t_f \\ \left[2.5 + \left(5 + \frac{8t * t_f}{5} \right) \cos \left(2\pi f_c t - \frac{\pi}{2} \right) \right] & , 0.5/t_f < t \leq 2.5/t_f \\ \left[2.5 - 2.5(t * t_f - 2.5) \right] & , 2.5/t_f < t \leq 3.5/t_f \end{cases}$$

$$z(t) = \begin{cases} 12t * t_f & , 0 < t \leq 2.5/t_f \\ \left[30 - 30(t * t_f - 2.5) \right] & , 2.5/t_f < t \leq 3.5/t_f \end{cases}$$

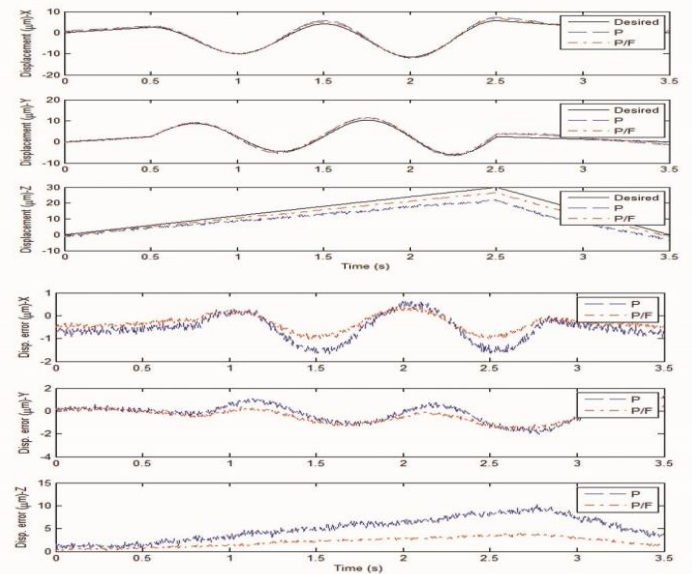
$$\theta_x(t) = \begin{cases} 0 & , 0 < t/t_f \leq 0.5/t_f \\ \left[\left(\frac{\pi}{72} \right) \sin(2\pi f_c t) \right] & , 0.5/t_f < t \leq 2.5/t_f \\ 0 & , 2.5/t_f < t \leq 3.5/t_f \end{cases}$$

$$\theta_y(t) = \begin{cases} 0 & , 0 < t \leq 0.5/t_f \\ \left[0.0436 + \left(\frac{\pi}{72} \right) \cos(2\pi f_c t) \right] & , 0.5/t_f < t \leq 2.5/t_f \\ 0 & , 2.5/t_f < t \leq 3.5/t_f \end{cases}$$

$$\theta_z(t) = \begin{cases} 0 & , 0 < t \leq 0.5/t_f \\ \left[\left(\frac{\pi}{144} \right) \sin(2\pi f_c t) \right] & , 0.5/t_f < t \leq 2.5/t_f \\ 0 & , 2.5/t_f < t \leq 3.5/t_f \end{cases}$$

Similarly, manipulating the same trajectory, the auxiliary factor is assigned by $t_f = 1, 10, 100$ for frequency (0.1, 1.0, 10)Hz, respectively, and the time span is (35, 3.5, 0.35) seconds.

The OptoForce 6-axis force/torque sensor mounted between the work parts and the robotic platform can quantify the interaction force and torque on the X, Y, and Z axes, respectively. Figures 23~24, and 26~27 show the tracking performance and tracking error of displacement and rotation, and Figures 25 and 28 show the measured interaction force/torque for each glass, and aluminum case, respectively. The average translation and orientation error norm for both controllers is listed in Table 9. As seen, the P/F controller, with support from the feedforward control to overcome variant manipulating speed, performs much better for machining all various work parts.

**Fig. 23. Tracking performance & error on X, Y, Z axis – Gls.**

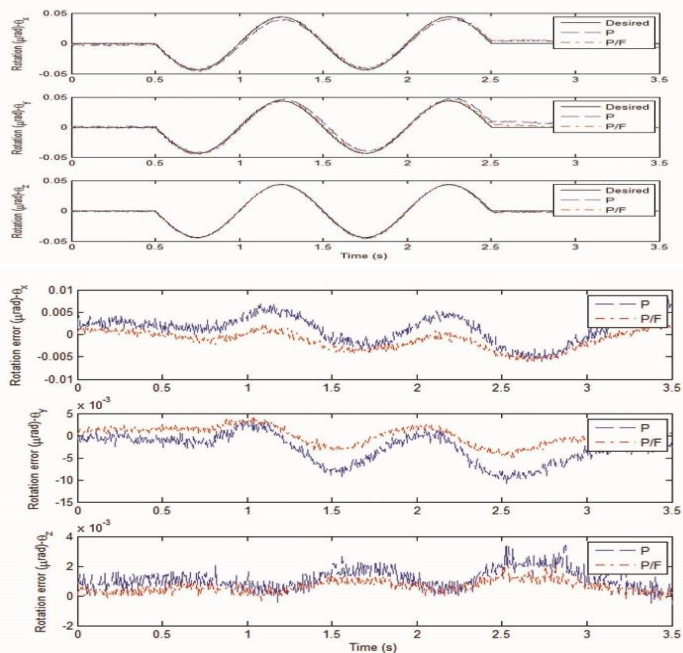


Fig. 24. Rotation tracking performance on $\theta_x, \theta_y, \theta_z$ – Gls.

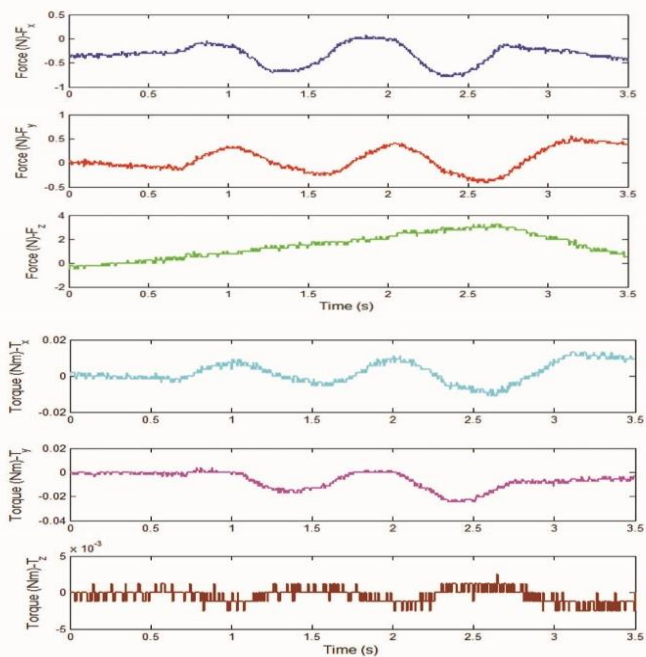


Fig. 25. Interaction force/torque on X, Y, Z axis – Gls.

Table 9. Tracking error – P controller & P/F controller.

work parts		glass	aluminum
P controller	translation error norm	5.702 μm	3.024 μm
	orientation error norm	0.028 μrad	0.014 μrad
P/F controller	translation error norm	0.988 μm	0.615 μm
	orientation error norm	0.0016 μrad	0.0069 μrad

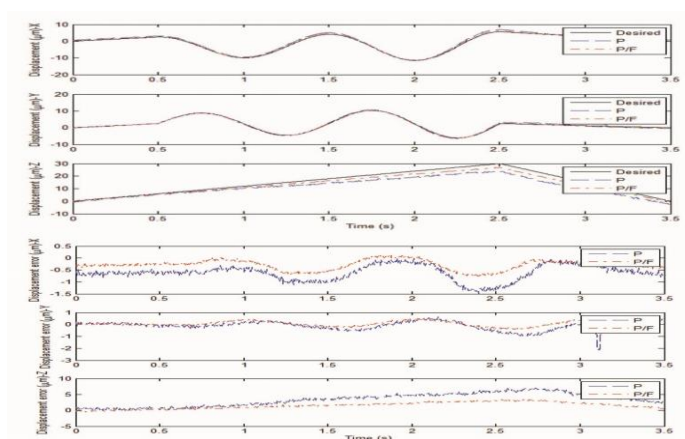


Fig. 26. Tracking performance & error X, Y, Z axis - Al.

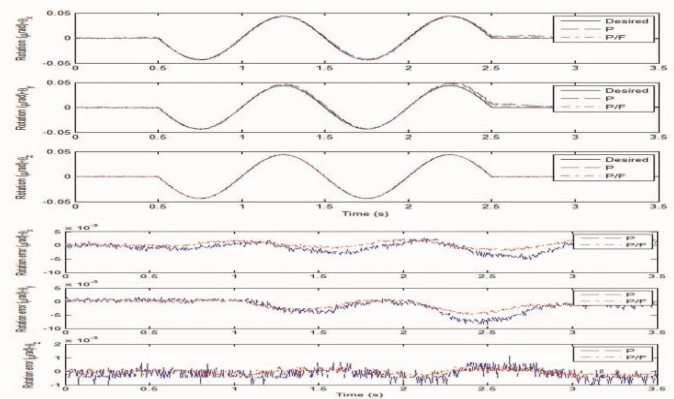


Fig. 27. Tracking performance & error on $\theta_x, \theta_y, \theta_z$ – Al.

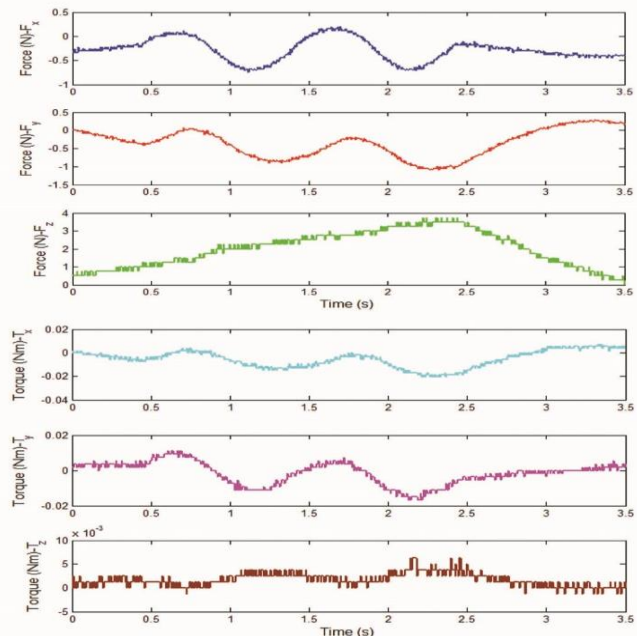


Fig. 28. Interaction force/torque on X, Y, Z axis – Al.

5. CONCLUSION

A 6DOF Stewart robotic platform with six piezo-driven leg actuators is established. With the derived dynamic modelling and the measurement method on the end effector, a task-space

control strategy that can reach the purpose of control on the end effector is practicable. The fundamental position tracking controller (P controller) is a computed-torque-based method associated with a PID. To deal with the hysteresis nonlinear effect of leg actuator is necessary to improve accuracy. As found, the hysteresis is variant to operating frequency and there exists an approximate linear relation between the leg displacement and the applied input voltage. Therefore, an attempt of using run-to-run adaptation scheme embedded on an internal model control associated with EWMA method is developed. The inverse Preisach hysteresis, the inverse Preisach model + EWMA, and the inverse Preisach model + PCC combined with the P controller are examined first on free space manipulation. As a result, the inverse Preisach model + PCC as a feedforward controller, combined with the position tracking controller, named P/F controller, achieves better performance. A further investigation is carried out on machining different work parts to include the stiffness control in the P and P/F controller. From experiment results, the P/F controller combines the position tracking control with the feedforward controller, notably outperforming the P controller. Using the P controller alone may not keep the target of nanoscale positioning at a low manipulating speed. The feedforward control is constructed with the Inverse Preisach model and an EWMA or PCC method integrated in a system of internal model control (IMC). The run-to-run IMC (RtR-IMC) discrete-time control scheme can adaptively tune the input/output relation, effectively dealing with the rate hysteresis effect. The proposed feedforward controller is simple and timesaving can integrate with a general position-tracking controller to significantly enhance performance and very instrumental to reduce the effort of building as well as executing an on-line control of a complex 6DOF Stewart platform.

ACKNOWLEDGEMENTS

The National Science Council funded this study under the grant NSC 101-2622-E-033-001-CC2, MOST105-2221-E-033-013, and Soundwide Technology Corp.

REFERENCES

- Ting, Y., Jar, H. C., & Li, C. C. (2007). Measurement and calibration for Stewart micromanipulation system. *Precision Engineering*, 31(3), 226-233.
- Lebret, G., Liu, K., & Lewis, F. L. (1993). Dynamic analysis and control of a Stewart platform manipulator. *Journal of Robotic Systems*, 10(5), 629-655.
- Dasgupta, B., & Mruthyunjaya, T. S. (1998). A Newton-Euler formulation for the inverse dynamics of the Stewart platform manipulator. *Mechanism and machine theory*, 33(8), 1135-1152.
- Jiles, D. C., & Atherton, D. L. (1984). Theory of ferromagnetic hysteresis. *Journal of applied physics*, 55(6), 2115-2120.
- Ge, P., & Jouaneh, M. (1997). Generalized Preisach model for hysteresis nonlinearity of piezoceramic actuators. *Precision engineering*, 20(2), 99-111.
- Yu, Y., Naganathan, N., & Dukkipati, R. (2002). Preisach modeling of hysteresis for piezoceramic actuator system. *Mechanism and Machine Theory*, 37(1), 49-59.
- Novak, M., Eichler, J., & Kosek, M. (2018). Difficulty in identifying Preisach hysteresis model weighting function using first-order reversal curves method in soft magnetic materials. *Applied Mathematics and Computation*, 319, 469-485.
- Novak, M., Eichler, J., & Kosek, M. (2018). Difficulty in identifying Preisach hysteresis model weighting function using first-order reversal curves method in soft magnetic materials. *Applied Mathematics and Computation*, 319, 469-485.
- Senjyu, T., Miyazato, H., Yokoda, S., & Uezato, K. (1998). Speed control of ultrasonic motors using neural network. *IEEE Transactions on Power Electronics*, 13(3), 381-387.
- Jung, H., & Gweon, D. G. (2000). Creep characteristics of piezoelectric actuators. *Review of Scientific Instruments*, 71(4), 1896-1900.
- Al Janaideh, M., Al Saaideh, M., & Rakotondrabe, M. (2020). On hysteresis modeling of a piezoelectric precise positioning system under variable temperature. *Mechanical Systems and Signal Processing*, 145, 106880.
- Li, K., Yang, Z., Lallart, M., Zhou, S., Chen, Y., & Liu, H. (2019). Hybrid hysteresis modeling and inverse model compensation of piezoelectric actuators. *Smart Materials and Structures*, 28(11), 115038.
- Ingolfsson, A., & Sachs, E. (1993). Stability and sensitivity of an EWMA controller. *Journal of Quality Technology*, 25(4), 271-287.
- Chen, A., Guo, R. S., Chou, Y. L., Lin, C. L., Dun, J., & Wu, S. A. (1999, October). Run-to-run control of CMP process considering aging effects of pad and disc. In *1999 IEEE International Symposium on Semiconductor Manufacturing Conference Proceedings (Cat No. 99CH36314)* (pp. 229-232). IEEE.
- Butler, S. W., & Stefani, J. A. (1994). Supervisory run-to-run control of polysilicon gate etch using in situ ellipsometry. *IEEE Transactions on Semiconductor Manufacturing*, 7(2), 193-201.
- Ting, Y., Li, C. C., & Lin, C. M. (2011). Controller design for high-frequency cutting using a piezo-driven microstate. *Precision engineering*, 35(3), 455-463.
- Salisbury, J. K. (1980, December). Active stiffness control of a manipulator in cartesian coordinates. In *1980 19th IEEE Conference on Decision and Control included the symposium on adaptive processes* (pp. 95-100).
- Ingolfsson, A., & Sachs, E. (1993). Stability and sensitivity of an EWMA controller. *Journal of Quality Technology*, 25(4), 271-287.
- Hunter, J. S. (1986). The exponentially weighted moving average. *Journal of quality technology*, 18(4), 203-210.
- Astrom, K. J. (1995). PID controllers: theory, design, and tuning. *The International Society of Measurement and Control*.
- Zamani, M., Karimi-Ghartemani, M., Sadati, N., & Parniani, M. (2009). Design of a fractional order PID controller for an AVR using particle swarm optimization. *Control Engineering Practice*, 17(12), 1380-1387.

Maiti, D., Acharya, A., Chakraborty, M., Konar, A., & Janarthanan, R. (2008, December). Tuning PID and PI/λ D δ controllers using the integral time absolute error criterion. In *2008 4th International Conference on Information and Automation for Sustainability* (pp. 457-462). IEEE.

Lewis, F. L., Dawson, D. M., & Abdallah, C. T. (2003). *Robot manipulator control: theory and practice*. CRC Press.

Appendix A. KINEMATICS AND DYNAMIC MODELLING

Kinematic formulation of a leg

The rotation matrix R_P of the centre point P_C concerning frame $\{B\}$ is defined by using Euler angle representation: firstly, rotating the moving frame $\{P\}$ w.r.t. the axis x_B of the fixed frame by an angle θ_x ; secondly, rotating w.r.t. the axis y_B by an angle θ_y ; and finally, rotating w.r.t. the axis z_B by an angle θ_z . Thus, the orientation transformation matrix can be derived as

$$R_P = \begin{bmatrix} C_{\theta_y}C_{\theta_z} & C_{\theta_y}C_{\theta_z}C_{\theta_x} - C_{\theta_y}C_{\theta_x} & C_{\theta_y}C_{\theta_z}C_{\theta_x} + C_{\theta_y}C_{\theta_x} \\ C_{\theta_y}C_{\theta_x} & C_{\theta_y}C_{\theta_z}C_{\theta_x} + C_{\theta_y}C_{\theta_x} & C_{\theta_y}C_{\theta_z}C_{\theta_x} - C_{\theta_y}C_{\theta_x} \\ -C_{\theta_y} & C_{\theta_y}C_{\theta_z} & C_{\theta_y}C_{\theta_x} \end{bmatrix} = \begin{bmatrix} u_x & v_x & \omega_x \\ u_y & v_y & \omega_y \\ u_z & v_z & \omega_z \end{bmatrix} \quad (\text{AI.1})$$

The close loop equation for each leg is defined by

$$\ell_i \hat{s}_i = P + R_P P_i - B_i \quad ; \quad i = 1, 2, \dots, 6 \quad (\text{AI.2})$$

where \hat{s}_i is the unit vector of the leg I defined as

$$\begin{bmatrix} r_{B_i}^{P_i} \end{bmatrix} / l_i = \begin{bmatrix} p_{x_i}^{B_i} & p_{y_i}^{B_i} & p_{z_i}^{B_i} \end{bmatrix}^T / l_i = \begin{bmatrix} \hat{s}_{x_i} & \hat{s}_{y_i} & \hat{s}_{z_i} \end{bmatrix}^T \quad \text{and} \\ B_i = \begin{bmatrix} r_B \cos(\lambda_i) & r_B \sin(\lambda_i) & 0 \end{bmatrix}^T \quad (\text{AI.3})$$

$$P_i = \begin{bmatrix} r_P \cos(\Lambda_i) & r_P \sin(\Lambda_i) & 0 \end{bmatrix}^T, \quad (\text{AI.4})$$

Differentiating (AI.2), the linear velocity of the leg is

$$\begin{bmatrix} \dot{r}_{B_i}^{P_i} \end{bmatrix} = \begin{bmatrix} \dot{r}_{B_C}^{P_C} \end{bmatrix} + \dot{R}_P \begin{bmatrix} r_{P_C}^{P_i} \end{bmatrix} + R_P \begin{bmatrix} \dot{r}_{P_C}^{P_i} \end{bmatrix} - \begin{bmatrix} \dot{r}_{B_C}^{B_i} \end{bmatrix} = \\ \begin{bmatrix} \dot{r}_{B_C}^{P_C} \end{bmatrix} + \begin{bmatrix} \dot{\omega}_i^x \end{bmatrix} R_P \begin{bmatrix} r_{P_C}^{P_i} \end{bmatrix} \quad (\text{AI.5})$$

where $\begin{bmatrix} \dot{r}_{B_C}^{B_i} \end{bmatrix} = \begin{bmatrix} \dot{r}_{P_C}^{P_i} \end{bmatrix} = 0$, and $\begin{bmatrix} \dot{\omega}_i^x \end{bmatrix}$ is a skew-symmetric matrix describing the leg's angular velocity w.r.t. the frame $\{B\}$

$$\begin{bmatrix} \dot{\omega}_i^x \end{bmatrix} = \begin{bmatrix} 0 & -\omega_z & \omega_y \\ \omega_z & 0 & -\omega_x \\ -\omega_y & \omega_x & 0 \end{bmatrix} \quad (\text{AI.6})$$

Differentiate (AI.5), the linear acceleration of the leg i is

$$\begin{bmatrix} \ddot{r}_{B_i}^{P_i} \end{bmatrix} = \begin{bmatrix} \ddot{r}_{B_C}^{P_C} \end{bmatrix} + \begin{bmatrix} \dot{\omega}_i^x \end{bmatrix} R_P \begin{bmatrix} r_{P_C}^{P_i} \end{bmatrix} + \\ \begin{bmatrix} \dot{\omega}_i^x \end{bmatrix} \left(\begin{bmatrix} \dot{\omega}_i^x \end{bmatrix} R_P \begin{bmatrix} r_{P_C}^{P_i} \end{bmatrix} \right) \quad (\text{AI.7})$$

where $\dot{\omega}_i$, describes the instantaneous change of the angular velocity of the leg w.r.t. the frame $\{B\}$ given by

$$\begin{bmatrix} \dot{\omega}_i \end{bmatrix} = \frac{d\omega_i}{dt} = \frac{\dot{s}_{i \times} \begin{bmatrix} r_{B_i}^{P_i} \end{bmatrix} + \hat{s}_{i \times} \begin{bmatrix} \ddot{r}_{B_i}^{P_i} \end{bmatrix}}{l_i} \quad (\text{AI.8})$$

A dynamic formulation of a leg

The kinetic energy of each leg with the summation of the fixed part and the extensible function is defined as

$$K_i = \frac{1}{2} \begin{bmatrix} \dot{r}_{B_i}^{P_i} \end{bmatrix}^T M_i \begin{bmatrix} \dot{r}_{B_i}^{P_i} \end{bmatrix} = \frac{1}{2} v_{s_i}^T m_{s_i} v_{s_i} + \\ \frac{1}{2} \omega_i^T I_{s_i} \omega_i + \frac{1}{2} v_{e_i}^T m_{e_i} v_{e_i} + \frac{1}{2} \omega_i^T I_{e_i} \omega_i \quad (\text{AI.9})$$

where v_{s_i} and v_{e_i} are the linear velocities of the fixed and extensible parts, respectively, given by

$$v_{s_i} = -\frac{l_{s_i}}{l_i} \hat{s}_{i \times} \begin{bmatrix} \dot{r}_{B_i}^{P_i} \end{bmatrix}; \quad v_{e_i} = -\frac{l_{e_i}}{l_i} \hat{s}_{i \times} \begin{bmatrix} \dot{r}_{B_i}^{P_i} \end{bmatrix} + \hat{s}_i \hat{s}_i^T \hat{s}_{i \times} \begin{bmatrix} \dot{r}_{B_i}^{P_i} \end{bmatrix} \quad (\text{AI.10})$$

$$\text{and} \quad \hat{s}_{i \times} = \begin{bmatrix} 0 & -\hat{s}_{z_i} & \hat{s}_{y_i} \\ \hat{s}_{z_i} & 0 & -\hat{s}_{x_i} \\ -\hat{s}_{y_i} & \hat{s}_{x_i} & 0 \end{bmatrix} \quad (\text{AI.11})$$

Summation of the inertia of fixed and extensible parts yields

$$I_{eq} = I_{s_i} + I_{e_i} = \text{diag}([I_s + I_i, I_s + I_i, 0]) \quad (\text{AI.12})$$

The kinetic energy of each leg is given by

$$K_i = \frac{1}{2} \begin{bmatrix} \dot{r}_{B_i}^{P_i} \end{bmatrix}^T \left(\frac{1}{l_i^2} m_{e_i} \begin{bmatrix} r_{B_i}^{P_i} \end{bmatrix}^T \begin{bmatrix} r_{B_i}^{P_i} \end{bmatrix} + m_{ce} \hat{s}_{i \times} \begin{bmatrix} \mathbf{AI.11} \end{bmatrix} \hat{s}_{i \times} \right) \begin{bmatrix} \dot{r}_{B_i}^{P_i} \end{bmatrix} \quad (\text{AI.12})$$

where $m_{ce} = (m_{s_i} l_{s_i}^2 + m_{e_i} l_{e_i}^2) / l_i^2$.

The mass matrix of each leg is derived as

$$M_i = \frac{1}{l_i^2} (m_{e_i} \begin{bmatrix} r_{B_i}^{P_i} \end{bmatrix}^T \begin{bmatrix} r_{B_i}^{P_i} \end{bmatrix} + (m_{s_i} l_{s_i}^2 + m_{e_i} l_{e_i}^2) \hat{s}_{i \times}^2 - l_{eq} \hat{s}_{i \times}^2) \quad (\text{AI.13})$$

The potential energy of each leg is determined as

$$P_i = -[0 \quad 0 \quad g]^T [m_{s_i} l_{s_i} \hat{s}_i + m_{e_i} (l_i - l_{e_i}) \hat{s}_i] \quad (\text{AI.14})$$

Using the Lagrange method, the relative derivative terms are described below.

The gravity vector G_i is determined by differentiating the potential energy w.r.t. The generalized coordinate is given by

$$G_i = \frac{\partial P_i}{\partial \begin{bmatrix} r_{B_i}^{P_i} \end{bmatrix}} = \left(\frac{1}{l_i} (m_{s_i} l_{s_i} \hat{s}_i + m_{e_i} (l_i - l_{e_i})) \hat{s}_{i \times}^2 - m_{e_i} \hat{s}_i \hat{s}_i^T \right)^T [0 \quad 0 \quad g] \quad (\text{AI.15})$$

The Coriolis and centrifugal vector is given by

$$C_i(\begin{bmatrix} r_{B_i}^{P_i} \end{bmatrix}, \begin{bmatrix} \dot{r}_{B_i}^{P_i} \end{bmatrix}) = \dot{M}_i \begin{bmatrix} r_{B_i}^{P_i} \end{bmatrix} - \\ \frac{1}{2} \frac{\partial}{\partial \begin{bmatrix} r_{B_i}^{P_i} \end{bmatrix}} (\begin{bmatrix} r_{B_i}^{P_i} \end{bmatrix}^T M_i \begin{bmatrix} r_{B_i}^{P_i} \end{bmatrix}) = -\frac{1}{l_i^2} \{ m_{e_i} l_{e_i} \begin{bmatrix} r_{B_i}^{P_i} \end{bmatrix}^T \hat{s}_{i \times}^2 \begin{bmatrix} r_{B_i}^{P_i} \end{bmatrix} - 2 l_i m_{b_i} \hat{l}_i \hat{s}_{i \times}^2 \} \text{ where} \\ m_{b_i} = \frac{1}{l_i} m_{e_i} l_{e_i} - \frac{1}{l_i^2} (l_{eq_i} + l_i^2 m_{ce_i}) \quad (\text{AI.16})$$

The dynamic equation of each leg is derived as

$$M_i \begin{bmatrix} \ddot{r}_{B_i}^{P_i} \end{bmatrix} + C_i \left(\begin{bmatrix} r_{B_i}^{P_i} \end{bmatrix}, \begin{bmatrix} \dot{r}_{B_i}^{P_i} \end{bmatrix} \right) + G_i = \mathcal{F}_i \quad (\text{AI.17})$$

Appendix B. EWMA AND PCC CONTROLLERS

The predictive model of a linear relation is defined by

$$\hat{Y}_{n+1} = \hat{\delta}_n + \hat{\rho}_{n+1} X_{n+1} \quad (\text{AII.1})$$

where \hat{Y}_{n+1} is the predictive output, whose value is expected to reach the target T after n runs nearly; parameters $\hat{\delta}$ and $\hat{\rho}$ Represent the estimated values of the actual δ and ρ in $Y_n = \rho_n X_n + \delta_n + d_n$ respectively. Following (AII.1), the input variable is defined as [17,18]

$$X_{n+1} = \frac{T - \hat{\delta}_n}{\hat{\rho}_{n+1}} \quad (\text{AII.2})$$

The estimated parameter can be adapted by using the following EWMA algorithm.

$$\hat{\delta}_n = \omega(Y_n - \hat{\rho}_n X_n) + (1 - \omega)\hat{\delta}_{n-1} \quad (\text{AII.3})$$

Where ω is the weighting factor in the range of [0,1].

The estimated parameter can be adapted by using the following PCC algorithm

$$X_{n+1} = \frac{T - \hat{\delta}_n - \hat{\phi}_n}{\hat{\rho}_{n+1}} \quad (\text{AII.4})$$

where the two parameters $\hat{\delta}$ and $\hat{\phi}$ is defined as

$$\hat{\delta}_n = \omega_1(Y_n - \hat{\rho}_n X_n) + (1 - \omega_1)\hat{\delta}_{n-1} \quad (\text{AII.5})$$

$$\hat{\phi} = \omega_2(Y_n - \hat{\rho}_n X_n - \hat{\delta}_{n-1}) + (1 - \omega_2)\hat{\phi}_{n-1} \quad (\text{AII.6})$$

ω_1 and ω_2 ($0 < \omega_1, \omega_2 < 1$) are the weights for (AII.5) and (AII.6), respectively, and $\hat{\phi}_n$ is used to compensate for the error incurred by $\hat{\delta}_n$.

For two successive runs expressed by (AII.3) in EWMA as well as (AII.5) and (AII.6) in PCC with the T replaced by Y in (AII.2) and (AII.4) for assumption not reaching the target yet, the estimated parameter is rewritten as

EWMA:

$$\begin{aligned} \hat{\delta}_n &= \omega(e_{n-1} + \hat{Y}_n - \hat{\rho}_n X_n) + (1 - \omega)\hat{\delta}_{n-1} \\ &= \omega(e_{n-1} + \hat{\delta}_{n-1}) + (1 - \omega)\hat{\delta}_{n-1} = \omega e_{n-1} + \hat{\delta}_{n-1} \end{aligned} \quad (\text{AII.7})$$

Where e_{n-1} is defined as the error between the actual output Y_n and the expected output \hat{Y}_n .

A discrete-time expression for (AII.7) is derived as

$$\hat{\delta}(z) = \left[\omega \frac{z^{-1}}{1-z^{-1}} \right] e(z) = G_E e(z) \quad (\text{AII.8})$$

PCC:

$$\hat{\delta}_n = \omega_1(e_{n-1} + \hat{Y}_n - \hat{\rho}_n X_n) + (1 - \omega_1)\hat{\delta}_{n-1} \quad (\text{AII.9})$$

$$= \omega_1 e_{n-1} + \omega_1 \hat{\phi}_{n-1} + \hat{\delta}_{n-1}$$

$$\begin{aligned} \hat{\phi}_n &= \omega_2(e_{n-1} + \hat{Y}_n - \hat{\rho}_n X_n - \hat{\delta}_{n-1}) + (1 - \omega_2)\hat{\phi}_{n-1} \\ &= \omega_2 e_{n-1} + \hat{\phi}_{n-1} \end{aligned} \quad (\text{AII.10})$$

A discrete-time expression for (AII.9) and (AII.10) is derived, respectively as

$$\hat{\delta}(z) = \frac{z^{-1}}{1-z^{-1}} [e(z) + \hat{\phi}(z)] \omega_1 \quad (\text{AII.11})$$

$$\hat{\phi}(z) = \frac{\omega_2 z^{-1}}{1-z^{-1}} e(z) \quad (\text{AII.12})$$

From (AII.11) and (AII.12), yields

$$\hat{\delta}(z) + \hat{\phi}(z) = \left[\omega_\Sigma \left(\frac{z^{-1}}{1-z^{-1}} \right) + \omega_\Pi \left(\frac{z^{-1}}{1-z^{-1}} \right)^2 \right] e(z) = G_E e(z)$$

where $\omega_\Sigma = \omega_1 + \omega_2$ and $\omega_\Pi = \omega_1 \omega_2$.

$$(\text{AII.13})$$

In Figure 5, the EWMA and PCC controllers can be defined in a discrete-time controller G_E . The tracking error checking to the input and disturbance, respectively, is defined as

EWMA:

$$\left. \frac{e^d(z)}{r^v(z)} \right|_{d=0} = \frac{(G_p - \hat{G}_p)(z-1)}{\hat{G}_p(z-1) + \omega G_p} = \frac{(\rho - \hat{\rho})(z-1)}{\hat{\rho}(z-1) + \omega \rho} \quad (\text{AII.14})$$

$$\left. \frac{e^d(z)}{d(z)} \right|_{r^d=0} = \frac{\hat{G}_p(z-1)}{\hat{G}_p(z-1) + \omega G_p} \quad (\text{AII.15})$$

PCC:

$$\left. \frac{e^d(z)}{r^v(z)} \right|_{d=0} = \frac{(\zeta - 1)(z-1)^2}{z^2 + (\lambda \omega_\Sigma - 2)z + \lambda(\omega_\Pi - \omega_\Sigma) + 1} \quad (\text{AII.16})$$

$$\left. \frac{e^d(z)}{d(z)} \right|_{r^v=0} = \frac{(z-1)^2}{z^2 + (\lambda \omega_\Sigma - 2)z + \lambda(\omega_\Pi - \omega_\Sigma) + 1} \quad (\text{AII.17})$$

where λ is the ratio of $\rho/\hat{\rho}$. The EWMA contains an integrator $1/(1-z^{-1})$; the PCC includes an integrator plus a double integrator that would be useful to adjust the parameter δ . Both can reach the target in case of no disturbance. The EWMA controller can overcome a step disturbance; however, the PCC controller can overcome both step and ramp disturbances.

According to the characteristic equations of (AII.14) and (AII.16), as well as the weights ($0 < \omega_1, \omega_2 < 1$) and ratio $\lambda > 0$, the stability of both EWMA and PCC controllers is defined by means of Jury stability test respectively as (Astrom 1995)

$$0 < \lambda = \frac{\rho}{\hat{\rho}} < 2 \quad \text{for EWMA} \quad (\text{AII.18})$$

$$\begin{cases} |\lambda(\omega_1 \omega_2 - \omega_1 - \omega_2) + 1| < 1 \\ \lambda \omega_1 \omega_2 > 0 \\ 4 + \lambda(\omega_1 \omega_2 - 2\omega_1 - 2\omega_2) > 0 \end{cases} \quad \text{for PCC} \quad (\text{AII.19})$$

Figure 29 shows the acceptable region of adaptation ratio λ corresponding to the weights ω_1 and ω_2 . As seen, if the estimated $\hat{\rho}$ is far from the actual ρ , i.e., λ becomes large, need to assign very small ω_1 and ω_2 to maintain stability.

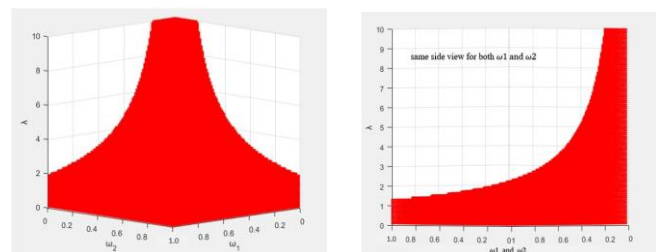


Fig. 29. Adaptation ratio λ vs. weights ω_1 and ω_2 .